Proceedings of the 3rd Marine Energy Technology Symposium
METS2015
April 27-29, 2015, Washington, D.C.

DEVELOPMENT OF A NUMERICAL WAVE TANK TO SUPPORT WETS ACTIVITIES

Krishnakumar Rajagopalan
ORE, University of Hawaii
Honolulu, HI, USA

Gérard Nihous
ORE, University of Hawaii
Honolulu, HI, USA

Luis Vega
HNEI, University of Hawaii
Honolulu, HI, USA

[1]Corresponding author: krishnak@hawaii.edu

BACKGROUND

The Hawaii Natural Energy Institute (HNEI) at the University of Hawaii has been tasked to help with the testing of Wave Energy Converters (WECs) of the Fixed Point Absorber (FPA) and Oscillating Water Column (OWC) types, at the U.S. Navy Wave Energy Test Site (WETS) located off Marine Corps Base Hawaii in Kaneohe (Oahu, Hawaii). In addition to field testing of WECs from different private developers, efforts are under way to enhance the capability of the WETS facility by providing guidance with the hydrodynamic design aspects of these machines. This would be accomplished with a suite of simple and high fidelity hydrodynamic numerical models.

Initial modeling efforts focused on linear potential flow theory that considers small amplitude waves and irrotational flow. This approach is often accurate enough in moderate operational seas. A couple of studies investigating interaction effects in large arrays of WEC devices [1,2] were completed to illustrate potential interferences among individual machines.

One study consisted of a theoretical determination of wave power extraction by arbitrary configurations of non-diffracting OWCs [1]. In the simplified framework where OWCs are modeled as structure-less pressure patches on the ocean surface, a mathematical solution for the overall potential flow from any wave farm was derived. Air compressibility in the OWC air chamber was included in the linearized equations. Wave spectral input typical of a particular site's wave climate was used. Switching from the linear frequency domain to the time domain, turbine efficiency which is a significant non-causal nonlinear effect could be represented. Hence, both pneumatic and mechanical turbine power could be evaluated. The algorithm was demonstrated for large arrays at two typical sites in Hawaiian waters. Results indicate the need for separations of the order of 3 to 5 OWC diameters, depending on array orientation, to limit interaction power losses to about 10%.

Another study considered very different WECs. WAMIT[3] was set up to analyze the hydrodynamic response of multiple slender articulated rafts consisting of floating cylindrical hinged segments [2]. These machines were modeled to represent the well-known Pelamis® P1-750 developed in Scotland, although the power take-off (PTO) adopted here was simply linear. The provision for hinge modes of motion already exists in WAMIT, and proved quite useful. It was extended to the case of multiple hinged bodies. Ultimately, the developer's recommendation to separate rows of such machines by half a length (75 m) and set the WECs a length apart (150 m) in any given row could be evaluated. Configurations were identified where more power could be produced than with the recommended spacing. These covered a significantly greater area, however, for power gains deemed marginal.

The outcome of this work demonstrated that available methods with modest computational needs may allow the estimation of WEC array performance. They also highlight the need to cast the issue of WEC interference in a greater context, since power output gains achieved at the expense of greater wave farm footprints are inherently problematic. From an infrastructural viewpoint, the costs of spreading WECs in space may be significant due to additional anchoring and power transmission constraints. Moreover, complex and potentially contentious permitting issues are likely to be exacerbated with larger wave farm footprints.

For deep water FPAs which use a submerged damping plate as reference for the PTO mechanism, the vortex shedding and the associated turbulence may become significant. Thus, in a wave field characterized by highly nonlinear waves (steep waves) and turbulence, the linear potential flow solutions may not be adequate. Under such circumstances, a high fidelity Computational Fluid Dynamics (CFD) solver or physical experiment becomes essential. The CFD solvers are formulated based on the Navier- Stokes equations with some turbulence modeling. As the complete flow domain (not just the boundaries) needs to be represented, however, the CFD solution typically requires substantial computational resources and time, unlike linear potential algorithms [4]. To bridge the gap between the less accurate but fast potential solvers and highly accurate but slow CFD solvers, *hydrid* methods are often used with inputs from potential solvers for wave diffraction and radiation coefficients on one hand, and from CFD solvers for drag coefficients on the other hand [4,5]. The drag coefficients can be evaluated from a carefully validated Numerical Wave Tank (NWT) using a CFD solver. Extreme conditions such as wave overtopping should entirely be modeled using CFD.

INTRODUCTION

In this paper, we focus our attention on the development and validation of a NWT using some geometries/shapes extensively found in WEC structures. We used the open source OpenFOAM CFD solver modified with a wave generation toolbox [6] to model the NWT. The geometries selected for validation of the NWT are the two-dimensional (2D) plates and three-dimensional (3D) disks as these may represent damper plates in deep water FPAs, and have been the subjects of extensive experimentation. This is followed by a descriptive section on the hybrid approach to WEC power prediction, before concluding remarks.

2D PLATE IN NWT

In the case of 2D plates submerged in an existing oscillatory flow, the seminal experiments of Keulegan and Carpenter [7] were simulated in a 2D NWT. As the Reynolds numbers of these experiments are small, no turbulence modeling was deemed necessary in the CFD solver. Second-order waves that were generated at one end of the NWT were reflected by the opposite wall to create a stationary wave field. The 2D plates were then located vertically at the nodes of the stationary wave field so that the flow was (predominantly) oscillating in the horizontal direction. Figure 1, shows the instantaneous positions of the free surface above the plate. About 125 time snapshots are included and are clearly representative of a well-established stationary wave field.

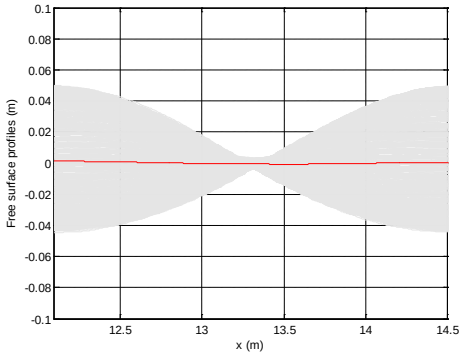

Figure 1. Free surface profiles above the plate location. A nodal region is established at x = 13.3 m. The red line represents the time average of the instantaneous free surface profiles. The 2D plate itself is located 0.25 m below the free surface. *x* and *y* are horizontal and vertical coordinates, respectively.

The important length scale, velocity and non-dimensional number that characterize the oscillating flow are the height of the plate, D, the amplitude of the oscillating velocity, U_m , the period of the wave field , T, and the Keulegan-Carpenter number, KC , defined as $U_m T/D$. Figure 2 shows the near field in the vicinity of the plate in the oscillating flow. The strong vortex shedding shown results in large drag coefficients and damping ratios for these shapes. By changing the height of the plates and the amplitude of the waves, which in turn changed U_m, total force measurements per unit plate width were obtained for a range of KC from 2 to 40. The pressure data on the plate was integrated to obtain the total force, F, on the plate.

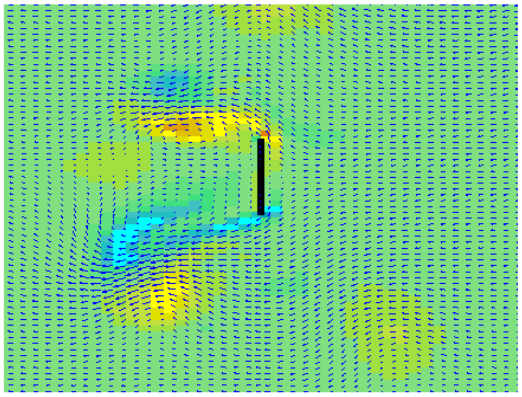

Figure 2. Vortex shedding from the plates at KC = 6.3. The color represents vorticity and the arrows represent velocity vectors.

Following Morison's equation [7] in oscillating flows, the total force can be decomposed into inertia component in phase with fluid acceleration and viscous term in phase with fluid velocity. Thus, in general form, we have:

$$F = \rho C_m A_o \frac{dU}{dt} + \frac{1}{2}\rho C_d D U |U| \qquad (1)$$

In Equation 1, the symbol U represents the horizontal velocity far removed from the object, and ρ the fluid density. A_o is defined as an equivalent circular area equal to $\pi D^2/4$. The symbols, C_m and C_d represent the inertia and drag coefficients respectively. In the present case, substituting $U = -U_m \cos\{(2\pi/T)t\}$ in Equation 1 and setting $\theta = (2\pi/T)t$ yields:

$$\frac{F}{\rho U_m^2 D} = \frac{\pi^2}{2KC} C_m \sin(\theta) - \frac{1}{2} C_d \,|\cos(\theta)|\cos(\theta) \qquad (2)$$

The MATLAB *fit* function was used to estimate the coefficients C_m and C_d from the normalized force data. Figure 3 shows the converged C_m and C_d data from the NWT experiments and the original experimental data of Keulegan and Carpenter [7]. There clearly is good agreement between the OpenFOAM numerical simulations and the experimental data.

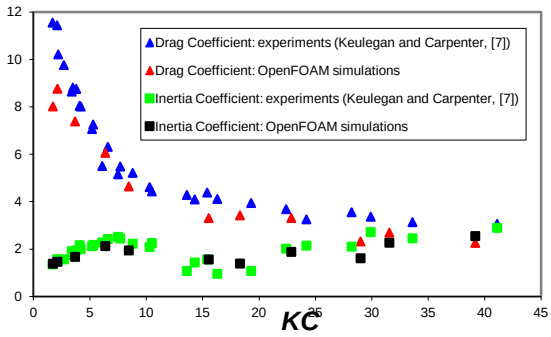

Figure 3. Comparison of drag and inertia coefficients (C_d and C_m) for 2-D plates: measurements (Keulegan and Carpenter, 1958), and estimates using OpenFOAM numerical wave tank.

3D PLATES IN NWT

Although the circular disk has a simple shape, experimental studies continue to this day to better estimate hydrodynamic coefficients in nonlinear regimes, such as, high KC [8], emphasizing the fact that predictions from linear potential theory may not be accurate enough in such cases. Consequently, we also considered numerical experiments in a 3D NWT, for oscillating circular disks at KC in the range 0.03 to 1.2, which represents a large departure from linear potential theory ($KC \approx 0$). For oscillating disks, KC is defined as $2\pi A/D$, where A is the amplitude of oscillation and D denotes the diameter of the plate. The frequency parameter, $\beta = fD^2/\nu$, where f denotes frequency of oscillation and ν the kinematic viscosity. Note that the Reynolds number Re is equal to $(KC)\beta$. In the results presented here, disk oscillations were imposed at 3 frequencies, namely 0.1, 0.5 and 1Hz.

The OpenFOAM CFD solver used for modeling the oscillating disk problem, *waveDyMFoam*, is a modified version of the standard *interDyMFoam* solver of Jacobsen *et al.* [6] that allows the computational mesh to be dynamically deformed in the presence of moving boundaries [9]. Turbulence quantities such as turbulent kinetic energy, k, and turbulence dissipation rate, ω are also computed (k-ω turbulence model) [6] whenever Re is above or near 10000.

Figure 4 shows the numerical grid for a circular disk of diameter 0.4 m and thickness 0.008 m.

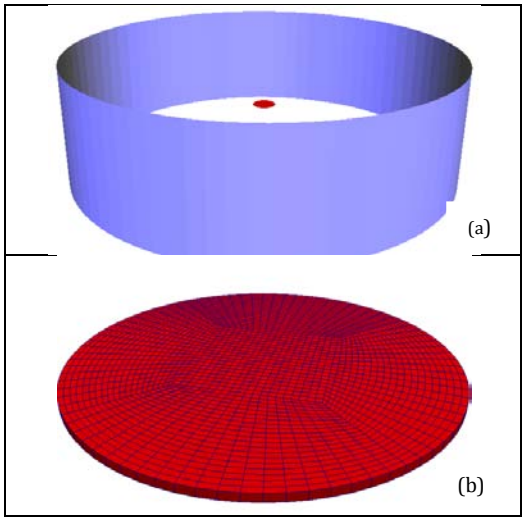

Figure 4. (a) Oscillating disk in red and the vertical boundary of the computational domain in blue. (b) Close up of the disk.

A Fourier analysis of the time histories of the force on the disk during several oscillation cycles yields the inertia and drag coefficients as shown below,

$$C_d = -\frac{3}{4\rho S U_m^2}\int_0^{2\pi} F(\theta)\cos(\theta)d\theta \qquad (3)$$

$$C_m = \frac{1}{\pi\rho\nabla U_m \omega}\int_0^{2\pi} F(\theta)\sin(\theta)d\theta \qquad (4)$$

In Equation 3, S denotes the projected area of the disk and equals $\pi D^2/4$. In Equation 4, ω is the circular frequency of oscillation. Since the drag coefficient is not well behaved at very low KC [10], results are presented in the form of a so-called linearized drag coefficient, C_b, defined as $C_d(KC)/4\pi$. Figure 5 shows the variation of C_b with KC from experiments and our numerical simulations.

According to Minamizawa and Endo [11], the drag data must become essentially independent of Re at high Re (for a given KC, a higher β corresponds to a higher Re). Thus, we should not expect a significant change in the drag coefficient as β rises. This trend is shown by the OpenFOAM numerical results. On the other hand, the experimental data shows large scatter. Also at low KC, viscous drag becomes negligible and the linearized drag coefficient must approach zero. This trend is also correctly shown by the OpenFOAM results.

The reduced added-mass coefficient A' is defined as $(\rho C_m \nabla)/(\frac{\rho D^3}{3})$, where $\rho C_m \nabla$ equals the added mass of the disk, $\frac{\rho D^3}{3}$ equals the theoretical added mass of the same disk in unbounded fluid considering potential flow and ∇ equals the displaced volume of the disk. Figure 6 compares this reduced added-mass coefficient from experiments and OpenFOAM numerical simulations. Although there is more scatter for the experimental data, there is generally good agreement between the data and numerical calculations. It is noteworthy that at large KC, say KC = 1.5, the value for A' predicted from linear potential theory would be 1, whereas it can be significantly higher, e.g. by 50% (see Figure 6). The inertia coefficient affects the natural period of a body and is therefore an important input in WEC design, for which resonance characteristics are critical.

HYBRID APPROACH TO WEC POWER PREDICTION

In an approach that we aim to follow for fast and numerically efficient WEC power predictions, the drag data will be obtained from CFD solvers. The behavior of the WEC in extreme seas will also be modeled with CFD. For extreme seas, an alternative and promising numerical method is the Smoothed Particle Hydrodynamics (SPH) [12], which is gridless due to its Lagrangian nature, and thus, may be more stable than standard Eulerian CFD models for handling extreme wave conditions.

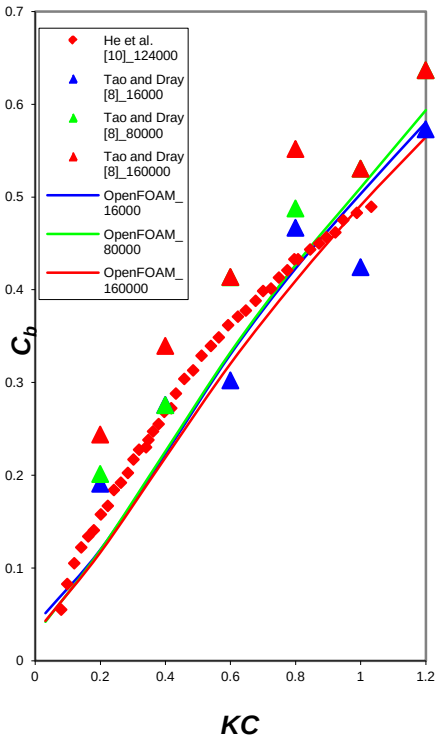

Figure 5. Selected experimental data and OpenFOAM numerical simulations for the linearized drag coefficient (C_b) of oscillating circular disks as a function of KC; numbers in the legend refer to β.

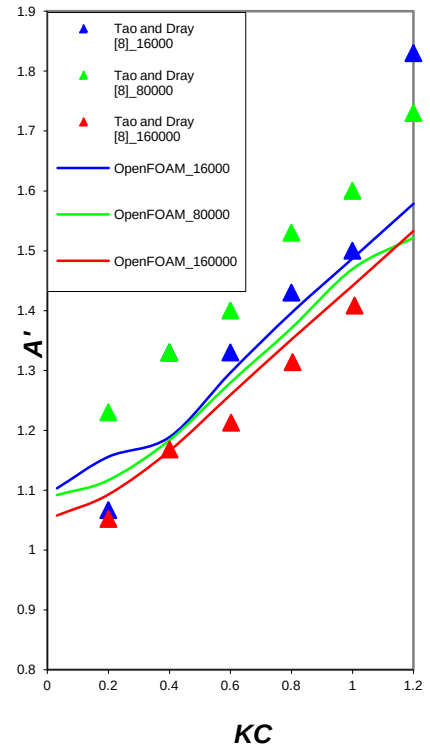

Figure 6. Selected experimental data and OpenFOAM numerical simulations for the reduced added-mass coefficient (A') of oscillating circular disks as a function of KC; numbers in the legend refer to β.

To fix ideas, with little loss of generality, we may write the uncoupled heave differential equation for a buoy-like WEC [13] as:

$$(M + \mu_\infty)\ddot{Z} = F_{ex} - \int_0^t K(t-\tau)\dot{Z}(\tau)dt + F_H + F_{PTO} + F_V \quad (5)$$

In Equation 5, $\ddot{Z}$ and $\dot{Z}$ are the heave acceleration and velocity, respectively. F_{ex}, μ_∞ and $K(t)$ represent, respectively, the wave excitation force, and the added mass and memory function from the wave radiation forces [13], all of which may be obtained from a linear potential flow solver such as WAMIT [3]. M, F_H, F_{PTO} and F_V denote, respectively, the mass of the WEC, the hydrostatic restoring force which depends on the wetted surface area, the PTO force which may include stiffness and damping components, and the viscous drag force which involves a drag coefficient (see Figure 5). Equation 5 can conveniently be solved in the time domain for each sea state, typically characterized by a significant wave height and peak period, to estimate the power output of the WEC equal to $C_{PTO}\dot{Z}_{PTO}^2$, where C_{PTO} is the damping coefficient of the PTO. These calculations would be repeated for different sea states to generate the power matrix of the WEC. An optimization of C_{PTO} in different sea states may be envisioned if practically achievable.

CONCLUSIONS

This paper outlines a suite of numerical methods developed to aid in the power prediction of WECs such as may be tested at WETS. The NWT developed with the open-source OpenFOAM CFD solver has been successfully validated with well-known experimental data. Currently, work is in progress to combine drag data from CFD/SPH, WAMIT output and wave climate data at the site into a single time domain framework, to efficiently predict WEC power performance.

ACKNOWLEDGEMENTS

This research was funded by a grant from the U.S. Department of Energy through the Hawaii National Marine Renewable Energy Center (Hawaii Natural Energy Institute, University of Hawaii).

REFERENCES

[1] Nihous, G.C., 2012. Wave power extraction by arbitrary arrays of non-diffracting oscillating water columns. Ocean Engineering 51, 94-105.
[2] Frederick, M., 2014. Hydrodynamic Modeling of Pelamis® P1-750 Wave Energy Converters using WAMIT software. Master of Science Plan B Research Paper, Dept. of Ocean and Resources Engineering, University of Hawaii, 60 pp.
[3] WAMIT™ software; WAMIT™ Incorporated; Chestnut Hill, Massachusetts; www.wamit.com
[4] Yu, Y., Li, Y. 2012. A synthesis of numerical methods for modeling wave energy converter-point absorbers. Renewable and Sustainable Energy Reviews 16, 4352-4364.
[5] Neary, V. S., Previsic, M., Jepsen, R. A., Lawson, M. J., Yu, Y.H., Copping, A. E., Fontaine, A. A., Hallett, K. C., Murray, D. K. 2014. Methodology for design and economic analysis of marine energy conversion (MEC) technologies. SANDIA REPORT
[6] Jacobsen, N. G., Fuhrman, D. R., Fredsøe, J., 2011. A wave generation toolbox for the open-source CFD library. Int. J. Numer. Methods Fluids 70(9), 1073-1088.
[7] Keulegan, G.H., Carpenter, L.H., 1958. Forces on cylinders and plates in an oscillating fluid. J. Res. Natl. Bur. Stand. 60(5), 423-440.
[8] Tao, L., Dray, D., 2008. Hydrodynamic performance of solid and porous heave plates. Ocean Eng. 35, 1008-1014.
[9] Jasak, H., Tuković, Ž, 2010. Dynamic mesh handling in OpenFOAM applied to fluid-structure interaction simulations. Proc. V Eur. Conf. Comput. Fluid Dyn. ECCOMAS CFD 2010, Lisbon, Portugal, 19 pp).
[10] He, H., Troesch, A.W., Perlin, M., 2007. Hydrodynamics of damping plates at small KC numbers. Proc. IUTAM Symp. Fluid Struct. Interact. Ocean Eng., Hamburg, Germany, 93-104.
[11] Minamizawa, M., Endoh, K., 1984. Fluid resistance on a disk oscillating in a liquid at rest. J. Chem. Eng. Japan 17(2), 186-191.
[12] Gesteira, M.G., Rogers, B.D., Dalrymple, R.A., Crespo, A.J.C., Narayanaswamy, M. 2010. User Guide for the SPHysics code.
[13] Babarit, A., Hals, J., Muliawan, M.J., Kurniawan, A., Moan, T., Krokstad, J. 2012. Numerical benchmarking study of a selection of wave energy converters. Renewable Energy 41, 44-63.